Electronic and Vibrational Properties of Porphycene Anions

Rabbani M. Gulam, Toshio Matsushita, and Junji Teraoka*

Graduate School of Science, Osaka City University, Sugimoto, Osaka 558-8585, Japan

Received: December 11, 2002

Resonance Raman spectra of the anion radical and dianion of a free-base porphycene are obtained, and quantum chemical calculations based on density functional theory methods are carried out in order to derive the force fields of porphycene anions. Normal modes with similar vibrational characteristics are correlated by examining the overlaps between the different redox states in order to characterize the frequency shifts measured for reduced porphycenes in certain skeletal vibrational modes. The observed resonance Raman behavior is generally consistent with the formation of the π anion radical and π dianion of *trans*-porphycene with C_{2h} symmetry upon reduction.

Introduction

Porphycene is a structural isomer of porphyrin, first synthesized by Vogel et al.[1,2] The molecular structure of free-base porphycene is thought to be a trans isomer with C_{2h} symmetry, while free-base porphyrin is a trans isomer with D_{2h} symmetry. It has been found that the ring system of various free-base porphycene derivatives undergo two reversible one-electron reductions with lower reduction potential compared to porphyrins.[3−5] Facile reduction of the porphycene ring must therefore be related to the small energy gap between the highest occupied molecular orbital (HOMO) and lowest unoccupied molecular orbital (LUMO) as a result of reduced symmetry, which is consistent with the longer wavelength shift of the first absorption maximum in porphycenes.[3] The first reduction species has been identified as a porphycene π anion radical by electron spin resonance (ESR) experiments.[6,7] However, the second reduced species has yet to be characterized.

Resonance Raman (RR) spectroscopy is a powerful tool for investigating the structure of porphyrin anion radicals.[8−14] Most of the Raman bands produced by skeletal vibrational modes shift to lower frequencies upon reduction, which has been rationalized as a first approximation on the basis of the nodal pattern of the e_g* molecular orbital in which the unpaired electron resides. Bocian et al. reported a markedly different RR spectrum for a free-base porphyrin anion radical compared to that for the neutral parent porphyrin and attributed the difference to vibronic coupling between the ground and low-lying excited states of the anion.[13] Upshifts have been observed for an anion radical of vanadylporphine, suggestive of B_{1g} distortion due to the Jahn−Teller effect.[15] However, apart from the present authors' previous report,[16] no detailed vibrational studies have been published for the porphycene anion radical and dianion, although the force field of the neutral parent porphycene has been determined theoretically and experimentally with special care taken with respect to tautomerism of the hydrogen atoms and hydrogen migration in the cavity of the molecule.[17,18]

In the previous letter,[16] the RR spectra of 2,7,12,17-tetra-*n*-propylporphycene (H_2TPrPc) was confirmed to exhibit various frequency shifts upon reduction, and the spectral behavior was found in general to agree with vibrational analysis based on density functional theory (DFT). Specifically, the observed frequency shifts of the porphycene skeletal vibrational modes roughly agreed with those calculated for the π anion radical and π dianion of porphycene without substituents (H_2Pc). However, there were considerable differences in RR frequencies between the calculations and experimental results for certain vibrational modes because the RR measurements were only performed for substituted porphycene.

The present report examines the RR spectra and DFT calculations of porphycenes in further detail as a continuation of previous work, representing a comprehensive study on the structures of porphycene anions. In the present analysis, RR spectra were measured for H_2Pc instead of H_2TPrPc, and multiple scaling factors were adopted for vibrational analysis of the neutral parent porphycene, the anion, and the dianion, because direct scaling of calculated vibrational frequencies using multiple scaling factors has been shown to be much more accurate than using a single scaling factor.[18,19] Finally, overlaps were completed between normal modes in different redox states to correlate the corresponding vibrational modes. This analysis gave a full characterization of the RR spectra of H_2Pc anions, and the procedure the present authors proposed here can be applied to interpret the frequency shifts for metal porphycenes and porphyrins that exhibit more complicated redox processes.

Experimental Section

General Procedures. Free-base H_2Pc was purchased from MDPI and used as received. H_2Pc was chemically reduced in tetrahydrofuran (THF) by contact with an Na mirror in a custom-made apparatus under a high vacuum of 6×10^{-6} Torr.[9] THF was thoroughly dehydrated with Na metal and degassed under high vacuum prior to use. The Na mirror was formed by distillation of solid Na metal under very clean conditions and high vacuum. Reduction steps were monitored by measuring absorption spectra (U-3000 spectrometer, Hitachi) using a 1 mm path length cuvette. Raman scattering was excited by a Kr^+ laser (2580, Spectra Physics) and recorded on a Raman spectrometer (400D, JEOL). Infrared (IR) spectra of the neutral parent were measured using a KBr disk (FT 7200, Hitachi).

Calculations. Ab initio calculations for H_2Pc based on DFT with B3LYP functional[20,21] were performed using the GAUSS-

* To whom correspondence should be addressed. E-mail: teraoka@sci.osaka-cu.ac.jp.

10.1021/jp027683k CCC: $25.00
Published on Web 03/11/2003

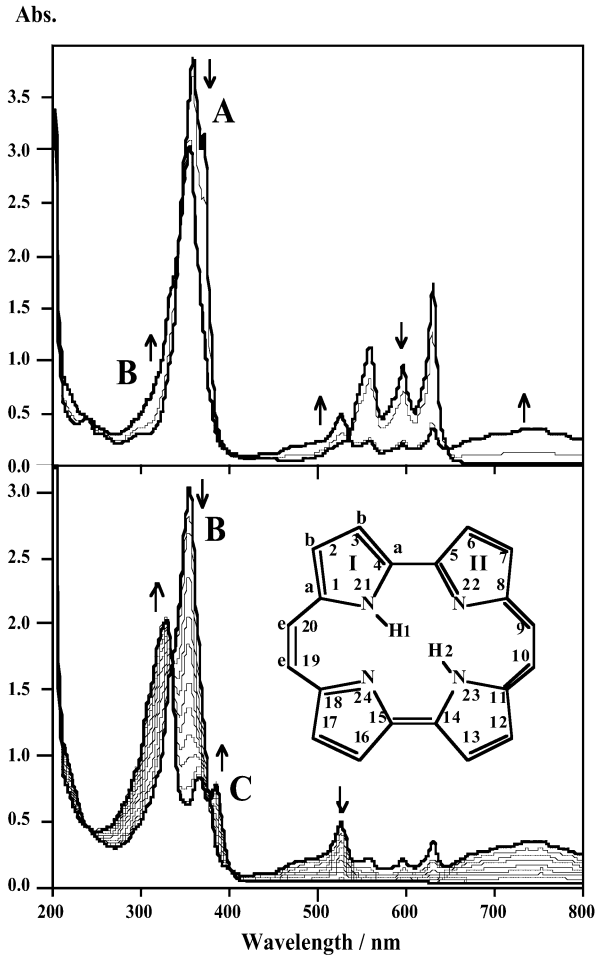

Figure 1. UV−vis absorption spectra for H_2Pc in THF upon successive contacts with Na mirror: (A to B) spectral changes concomitant with the first reduction stage; (B to C) spectral changes concomitant with the second reduction stage. Inset: Schematic molecular structure of H_2Pc and labeling of atoms.

IAN 98 program package[22] with the 6-31G(*d*) basis set.[23] All geometries were fully optimized at that level, and multiple scaling factors were used for correction of the calculated frequencies to those observed.[19,24] Normal coordinate analysis based on DFT was carried out for the free-base porphycene, the anion radical, and the dianion species in order to explain the frequency shifts of Raman bands upon chemical reduction. This kind of frequency calculation has only been performed to date for the neutral parent.[17,18] Vibrational correlations for each vibrational mode were estimated by taking the dot products (overlap) of every combination of normal modes in two different redox states.

Results

The upper panel in Figure 1 shows the successive changes in electronic absorption spectra of H_2Pc upon contact with the Na mirror. As the contact time increased, five strong absorption bands (358, 371, 558, 597, and 630 nm) became weaker, while two weak bands (526 and around 740 nm) became stronger. Well-defined isosbestic points were obtained at 342, 395, 534, and 645 nm. The Soret band weakened by 25%, which is much less than in the case of H_2TPrPc (50%).[16] The lower panel shows the subsequent changes in the absorption spectra upon further contact with Na mirror. The bands at 328 and 384 nm intensified while the absorption intensity of the other bands decreased gradually until the peaks finally disappeared. Well-defined

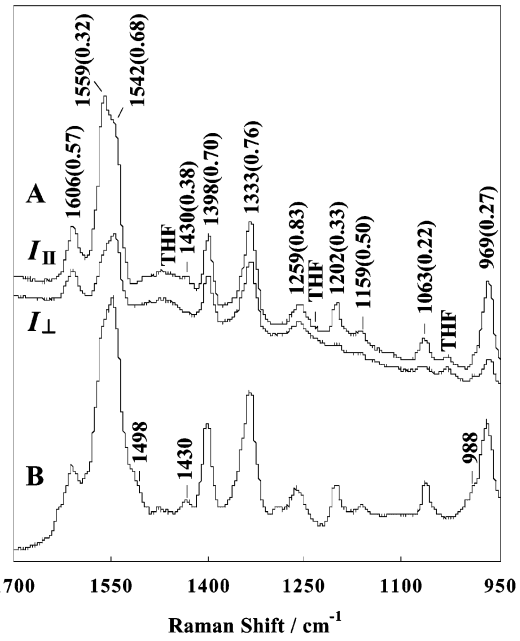

Figure 2. Resonance Raman spectra for H_2Pc neutral parent. Polarized spectra (A) were measured in THF, and spectrum B was measured in CCl_4. Depolarization ratios are given in parentheses. Excitation laser power was 6 mW at 406.7 nm.

isosbestic points were obtained at 334, 376, and 400 nm. Given the well-defined isosbestic points in the spectra, it is suggested that each spectral change results from the population change of two redox components. The chemical species that yielded spectra A−C shall hereafter be referred to as the neutral parent, the anion, and the dianion species, respectively.

The neutral parent attached to the Na mirror will be reduced instantly to the final dianion species even if in contact for only a short time because of the high redox potential of the Na mirror. Reaction will then proceed between the dianion and neutral bulk, resulting in chemical equilibrium between the neutral and the anion. The successive reduction process can also be understood in terms of this mechanism. The spectra of these redox states are almost identical to those obtained in previous studies.[5] Furthermore, the dianion sample reverted to the parent porphycene upon exposure to air, with ca. 95% recovery. It therefore appears that two redox equilibria were monitored in a stepwise relationship.

Figure 2A shows the polarized RR spectra of the neutral parent H_2Pc in THF, in which five depolarized Raman bands and other polarized bands were observed. The RR spectrum of the same sample in CCl_4 was also measured in order to resolve any Raman bands obscured by the THF bands in Figure 2A, and the results are shown in Figure 2B. Raman bands can be seen at 1498, 1430, and 988 cm^{-1}.

Figure 3 shows the RR spectra for H_2Pc in THF during reduction by the Na mirror. The redox states in the RR spectra correspond to the absorption spectra shown in Figure 1. The RR spectra B and C were obtained after subtraction of the contribution from the solvent and various species such that each spectrum describes only the redox species, anion or dianion porphycene. The correspondence between bands of these species were tentatively determined by careful comparison of the successive RR spectra (data not shown). Final determination will be discussed after theoretical calculations. However, it is worthwhile here to note the frequency shifts for certain skeletal vibrational modes upon reduction of H_2Pc, just as seen in the experimental data. The most intense Raman band at 1559 cm^{-1}

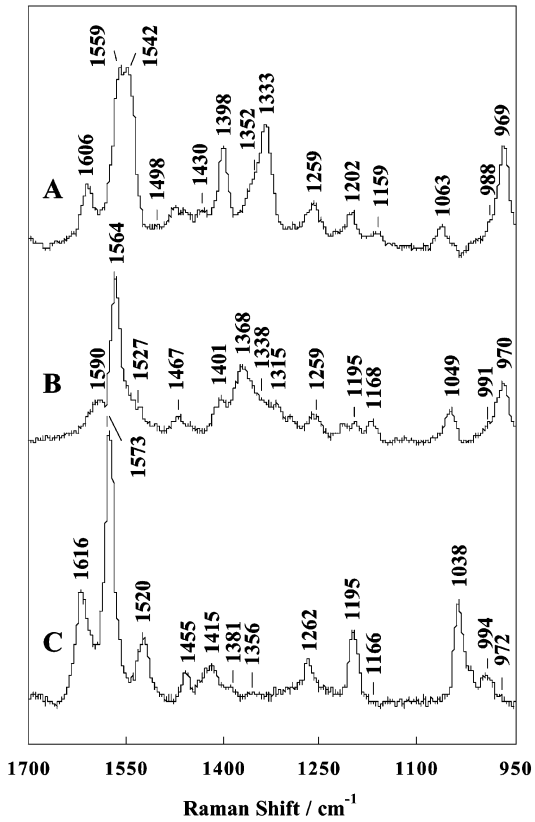

Figure 3. Resonance Raman spectra for H_2Pc in THF upon reduction using an Na mirror. Spectra A−C correspond to the neutral parent, the anion, and the dianion porphycenes. Excitation laser power was 6 mW at 406.7 nm.

shifted continuously to higher frequencies with almost unchanged intensity, while the 1542 cm^{-1} band appeared to shift to lower frequencies with considerable loss of intensity. The Raman band at 1606 cm^{-1} underwent a downshift for the anion and an upshift for the dianion. The 1398 cm^{-1} band shifted in a similar manner, down to 1368 and up to 1381 cm^{-1}, but with a more pronounced decrease in intensity. The band at 1063 cm^{-1} shifted continuously to lower frequencies and increased in intensity, while the 969 cm^{-1} band exhibited very little shift but a considerable loss of intensity. The counterpart of the band at 1333 cm^{-1}, shifted to 1315 cm^{-1} in the anion, is missing in the dianion. Normal-mode analysis of H_2Pc in each redox state will be required in order to interpret these frequency shifts.

There are 54 gerade and 54 ungerade vibrations ($37A_g + 17B_g + 18A_u + 36B_u$) under C_{2h} symmetry, where the A_g and B_u modes are in-plane vibrations, the A_g and B_g vibrations are Raman-active, and A_u and B_u are IR-active. The frequencies of all 108 vibrations of the neutral parent H_2Pc were scaled using multiple scaling factors as proposed by Pulay et al.,[19] and the results are listed in Table 1. The presented frequencies are almost identical to the multiple scaled frequencies calculated by Kozlowski et al.[18] and closely match the experimental data except for three IR-active bands, $18A_u$ (20 cm^{-1} difference), $21B_u$ (12 cm^{-1}), and $27B_u$ (17 cm^{-1}), and a Raman active band, $19A_g$ (12 cm^{-1}). It should be stressed that, for the first time, the frequencies of the anion and the dianion have been successfully calculated by DFT methods using the same multiple scaling factors as those for the neutral parent. These frequencies are given in Table 1 together with the vibrational frequencies for the neutral parent. The normal modes with similar vibrational characteristics were correlated for the different redox states by examining overlaps. The dot products ($\mathbf{Q}_{nj}$, $\mathbf{Q}_{mk}$), where $\mathbf{Q}_{nj}$ is the nth normal mode of the jth redox state and $\mathbf{Q}_{mk}$ is the mth normal mode of the kth redox state, were calculated, and a set of Raman bands with the largest overlaps was chosen as a final set of correlated vibrations for the normal mode. The values of $|(\mathbf{Q}_{nj}, \mathbf{Q}_{nk})|^2$ are shown in parentheses in Table 1. The $10A_g$ mode of the neutral parent at 969 cm^{-1}, for example, has 100% overlap with the anion, indicating that the vector is parallel to that for the 974 cm^{-1} band of the anion. The overlap between the neutral parent and the anion is considerably smaller for the $23A_g$ mode, which in the anion corresponds to an almost equal composition of $22A_g$ (34%) and $23A_g$ (36%) of the neutral with smaller components of $24A_g$ (18%) and $25A_g$ (10%). The situation is more complicated for the 28-, 29-, and $30A_g$ modes. The $28A_g$ (32% with $29A_g$) and $29A_g$ modes (42% with $28A_g$) in the neutral parent mix to produce new normal modes in the anion. The new $29A_g$ (24% with $30A_g$) and $30A_g$ (24% with $29A_g$) in the anion then couple in the dianion state. This vibrational mixing of $28A_g$ and $29A_g$ modes is thought to be responsible for the considerable weakening of the $28A_g$ mode in the anion spectrum.

A summary of the bond lengths and angle of the neutral parent and its anion and dianion in Table 2 allows the frequency shifts upon reduction to be related to the structural parameters of the main ring. The parameters of the neutral parent are exactly the same as the B3-LYP/6-31G(*d*) values calculated by Kozlowski et al.,[18] some of which differ considerably from the experimental bond distances.[1] This is the first report of the geometrical parameters of the anions. Upon reduction, the bond lengths varied alternately around the porphycene outer ring, shown as the values in parentheses in Table 2. The $C_{a-}N$ bond on the other hand exhibited a small increase. The changes in bond lengths resulting from the second reduction followed a trend similar to that of the first reduction. It will be discussed later whether the frequency shifts upon reduction can be evaluated using the geometrical parameters. It should be noted here that the porphycene core consisting of four nitrogen atoms expands significantly upon reduction (see $r(N_{21}N_{22})$ and $r(N_{22}N_{23})$ in Table 2). As a result, the inner NH−N distances become longer, yet the difference between $N_{21}H-N_{22}$ and $N_{21}H-N_{24}$ is still considerable, such that the symmetry of anions remains C_{2h} and does not change to D_{2h}, which would have occurred if symmetrical $N_{21-}H-N_{24}$ and $N_{22-}H-N_{23}$ bonds had formed.

Discussion

Raman Behavior upon Reduction. A total of 14 sets of skeletal Raman bands were obtained for H_2Pc in different redox states, and the Raman frequencies observed were found to be very similar to those observed by Fourier transform (FT) Raman spectroscopy[17] except for an extra band at 1352 cm^{-1}.

The observed RR frequencies taken from Figure 3 are listed in Table 3 for comparison with calculated frequencies of the corresponding Raman active modes selected from Table 1. The theoretical modes corresponding to the observed bands were chosen first on the basis that the frequencies of the neutral parent should be close to those observed and second on the patterns of calculated frequency shifts, which must be similar to those of the observed frequencies for the various redox states. The observed RR frequencies were readily related to the calculated frequencies as a one-to-one correspondence because the correction using multiple scaling factors predicted the experimental results with good accuracy. Almost all band correspondences for the neutral parent are consistent with those found in the previous study.[18] The only exception is the choice of $19A_g$ for the 1259 cm^{-1} band, with frequencies differing by 12 cm^{-1}.

TABLE 1: Vibrational Frequencies ($\tilde{\nu}$/cm^{-1}) of *trans*-H_2Pc and Its Reduced Forms Derived from MO Calculations Using Six Scaling Factors[a]

symmetry	neutral	anion[b]	dianion[c]	symmetry	neutral	anion[b]	dianion[c]
$1A_u$	60	57 (100)	49 (100)	$10A_g$	969	974 (100)	977 (96)
$2A_u$	70	67 (100)	63 (100)	$11A_g$	976	989 (96)	991 (90)
$3A_u$	86	92 (100)	99 (100)	$12A_g$	989	996 (98)	1000 (92)
$1B_g$	116	99 (100)	77 (100)	$11B_u$	1003	1003 (98)	1001 (96)
$2B_g$	130	131 (100)	132 (100)	$12B_u$	1047	1032 (94)	1016 (46)
$1A_g$	149	148 (100)	146 (100)	$13A_g$	1055	1035 (94)	1014 (92)
$2A_g$	192	184 (100)	177 (100)	$13B_u$	1058	1038 (98)	1022 (48)
$3B_g$	193	194 (96)	193 (100)	$14A_g$	1061	1045 (94)	1028 (92)
$4A_u$	199	186 (98)	171 (98)	$14B_u$	1090	1096 (96)	1098 (100)
$4B_g$	204	209 (96)	213 (100)	$15A_g$	1109	1111 (98)	1109 (98)
$1B_u$	236	236 (100)	240 (100)	$16A_g$	1153	1161 (96)	1160 (96)
$5A_u$	303	301 (76)	291 (96)	$15B_u$	1172	1182 (66)	1180 (94)
$6A_u$	312	319 (76)	325 (96)	$16B_u$	1190	1192 (67)	1183 (98)
$2B_u$	321	318 (100)	314 (100)	$17A_g$	1208	1203 (100)	1199 (100)
$3A_g$	342	338 (100)	332 (100)	$17B_u$	1231	1229 (88)	1225 (92)
$4A_g$	365	364 (100)	362 (100)	$18A_g$	1254	1244 (90)	1231 (90)
$3B_u$	386	381 (100)	374 (100)	$18B_u$	1257	1273 (62)	1283 (64)
$5B_g$	389	379 (98)	363 (100)	$19A_g$	1271	1272 (92)	1273 (96)
$4B_u$	470	467 (100)	464 (100)	$19B_u$	1289	1296 (56)	1332 (28)
$6B_g$	480	482 (100)	475 (98)	$20B_u$	1306	1307 (83)	1343 (74)
$5A_g$	491	489 (100)	485 (100)	$20A_g$	1337	1318 (56)	1303 (86)
$7A_u$	499	489 (100)	474 (98)	$21A_g$	1349	1343 (69)	1355 (64)
$6A_g$	603	600 (100)	595 (100)	$21B_u$	1368	1379 (49)	1388 (71)
$5B_u$	618	618 (100)	616 (100)	$22B_u$	1373	1355 (74)	1308 (56)
$8A_u$	625	628 (90)	622 (88)	$22A_g$	1375	1369 (38)	1322 (52)
$7B_g$	628	631 (94)	625 (74)	$23A_g$	1396	1376 (36)	1382 (77)
$8B_g$	658	647 (92)	639 (67)	$24A_g$	1407	1407 (58)	1413 (85)
$9A_u$	658	654 (90)	652 (77)	$23B_u$	1414	1394 (49)	1415 (59)
$7A_g$	665	656 (100)	645 (100)	$25A_g$	1437	1418 (67)	1424 (83)
$6B_u$	669	661 (100)	652 (100)	$24B_u$	1458	1423 (69)	1404 (72)
$10A_u$	696	685 (94)	659 (62)	$25B_u$	1466	1465 (77)	1458 (59)
$9B_g$	697	683 (66)	656 (76)	$26B_u$	1486	1473 (85)	1477 (67)
$10B_g$	701	689 (72)	670 (71)	$26A_g$	1494	1467 (85)	1445 (86)
$11A_u$	710	693 (96)	677 (74)	$27A_g$	1518	1492 (79)	1474 (90)
$12A_u$	745	709 (100)	669 (86)	$27B_u$	1527	1522 (78)	1556 (49)
$11B_g$	755	724 (83)	688 (56)	$28A_g$	1543	1523 (52)	1508 (92)
$12B_g$	768	731 (88)	698 (62)	$29A_g$	1561	1562 (52)	1568 (71)
$13A_u$	776	743 (94)	730 (44)	$28B_u$	1563	1572 (77)	1596 (71)
$13B_g$	812	773 (92)	751 (49)	$29B_u$	1582	1541 (76)	1512 (79)
$14A_u$	815	774 (94)	712 (18)	$30A_g$	1604	1594 (86)	1604 (74)
$8A_g$	832	832 (98)	829 (100)	$30B_u$	2912	2944 (100)	2966 (96)
$7B_u$	837	836 (100)	833 (100)	$31A_g$	2914	2945 (100)	2961 (98)
$15A_u$	868	797 (98)	708 (67)	$31B_u$	3032	2996 (100)	2948 (96)
$14B_g$	869	799 (96)	715 (77)	$32A_g$	3032	2996 (100)	2948 (98)
$15B_g$	877	807 (88)	730 (40)	$32B_u$	3050	3020 (100)	2981 (100)
$16A_u$	879	808 (94)	752 (50)	$33A_g$	3050	3021 (100)	2981 (100)
$9A_g$	880	888 (100)	896 (100)	$34A_g$	3101	3070 (100)	3026 (100)
$16B_g$	888	888 (94)	895 (98)	$33B_u$	3101	3070 (100)	3026 (100)
$8B_u$	898	903 (100)	908 (100)	$34B_u$	3116	3091 (96)	3054 (62)
$9B_u$	924	953 (77)	972 (58)	$35A_g$	3116	3091 (98)	3054 (62)
$17A_u$	933	911 (98)	893 (100)	$35B_u$	3121	3094 (96)	3056 (62)
$17B_g$	934	912 (98)	893 (98)	$36A_g$	3121	3094 (98)	3056 (62)
$10B_u$	939	962 (76)	977 (56)	$36B_u$	3133	3111 (100)	3083 (100)
$18A_u$	947	947 (100)	951 (100)	$37A_g$	3133	3112 (100)	3083 (100)

[a] Stretches: X−X, 0.9207; C−H, 0.9164; N−H, 0.9242. Bends: X−X−H, 0.9431; X−X−X, 1.0144. Torsions: 0.9523, where X is C or N. Values in parentheses are percentages of vibrational overlap. [b] Between normal modes of the neutral and anion. [c] Between the anion and dianion in the same row.

Kozlowski et al.[18] previously assigned this band to $18A_g$ (1254 cm^{-1}), the frequency of which is close to the observed. However, $19A_g$ was chosen here because the pattern of $19A_g$ frequency shifts is consistent with the behavior of the 1259 cm^{-1} band. Theoretical calculations were helpful in determining band correspondences across the various redox states: without prediction, it would have been hard to ascertain that the Raman band at 1542 cm^{-1}, for example, shifted to a weak band at 1527 cm^{-1} and then 1520 cm^{-1} upon reduction, even though the successive RR spectra were examined carefully. Different types of frequency shifts were observed upon reduction; monotonic downshifts, upshifts, down- and upshifts, and minor shifts. For all the cases, theoretical calculations are generally in good agreement with both the direction and magnitude of the shift. An interesting shift pattern is the down- and upshift of Raman bands such as $21A_g$, $23A_g$, $25A_g$, and $30A_g$. Even for these unusual shifts, theoretical calculations predicted the patterns very well.

The RR spectra of M(TPrPc), where M = Fe, Co, Ni, Cu, have been reported, and certain normal modes have been tentatively assigned to local vibrations based on isotope shifts.[25] Recently, the present authors reported the RR spectra of H_2-TPrPc in different redox states and assigned Raman bands with the aid of molecular orbital (MO) calculations.[16] Those assign-

TABLE 2: Main Ring Parameters for Stationary Points on the Trans Neutral Parent Porphycene, the Anion (H_2Pc^-), and the Dianion (H_2Pc^{2-})[a]

parameter[b]	H_2Pc	H_2Pc^- ($\Delta^c \times 10^2$)	H_2Pc^{2-} ($\Delta^d \times 10^2$)
$r(C_1C_2)$	1.435	1.416(−2)	1.401(−2)
$r(C_2C_3)$	1.378	1.398(+2)	1.418(+2)
$r(C_3C_4)$	1.431	1.415(−2)	1.401(−1)
$r(C_4C_5)$	1.413	1.434(+2)	1.458(+2)
$r(C_5C_6)$	1.450	1.433(−2)	1.416(−2)
$r(C_6C_7)$	1.365	1.383(+2)	1.403(+2)
$r(C_7C_8)$	1.456	1.436(−2)	1.418(−2)
$r(C_8C_9)$	1.413	1.430(+2)	1.447(+2)
$r(C_9C_{10})$	1.394	1.380(−1)	1.369(−1)
$r(C_{10}C_{11})$	1.408	1.428(+2)	1.447(+2)
$r(C_1N_{21})$	1.367	1.372(+1)	1.377(+1)
$r(N_{21}C_4)$	1.364	1.367(0)	1.372(+1)
$r(C_5N_{22})$	1.353	1.355(0)	1.359(0)
$r(N_{22}C_8)$	1.361	1.367(+1)	1.373(+1)
$r(N_{21}H_1)$	1.043	1.041(0)	1.041(0)
$r(N_{22}H_1)$	2.655	2.675(+2)	2.700(+3)
$r(N_{22}H_2)$	1.722	1.754(+3)	1.790(+4)
$r(N_{21}N_{22})$	2.826	2.850(+2)	2.878(+3)
$r(N_{22}N_{23})$	2.684	2.715(+3)	2.753(+4)
$\angle(C_4N_{21}H_1)$	128.2	128.0	128.0
$\angle(C_5N_{22}H_2)$	140.6	140.8	141.2
$\angle(C_1N_{21}C_4)$	111.0	111.1	111.2
$\angle(N_{21}C_4C_5)$	121.7	121.7	121.7
$\angle(C_4C_5N_{22})$	121.0	121.0	121.0
$\angle(C_5N_{22}C_8)$	106.9	106.9	107.0
$\angle(N_{22}C_8C_9)$	126.3	125.8	125.3
$\angle(C_8C_9C_{10})$	132.1	132.8	133.6
$\angle(C_9C_{10}C_{11})$	131.2	131.6	132.0
$\angle(C_{10}C_{11}N_{23})$	125.7	125.1	124.7

[a] Only half of the total main ring parameters are displayed because of symmetry. [b] Bond lengths in angstroms and bond angles in degrees. [c] Bond length difference between the neutral parent and the anion. [d] Bond length difference between the anion and the dianion.

ments are basically the same as in the present case for H_2Pc. A set of atoms that dominated displacements in the normal mode in each redox state was selected, and the dot products (**q**, **Q**) were evaluated, where **q** is the displacement vector of one of the selected atoms for a normal mode **Q**. The dot product can be used to characterize the participation of a motion of the atom in the normal vibration.

The selected atoms are listed in Table 3, along with percentages for the summation of (**q**, **Q**) for the set of focused atoms in each redox state. The displacements in Table 3 can be utilized for the approximate characterization of a vibration and are useful for interpreting the frequency shifts in terms of alterations of bond length upon reduction. Furthermore, this approach has the advantage over the conventional potential energy distribution method that no unfavorable off-diagonal terms arise and most of the significant contributions are found to be positive. It should be noted that the sum of all values is unity by definition. The $30A_g$ mode includes primary $\nu(C_aC_a)$ stretching, changing to $\nu(C_eC_e)$ stretching to reflect the lower level of overlap in the dianion. The $29A_g$ mode is derived predominantly from $\nu(C_aC_e)$, with a minor contribution from $\nu(C_eC_e)$ stretching in the neutral parent, but $\nu(C_eC_e)$ becomes dominant for the $29A_g$ mode in both the anion and dianion. On the other hand, $28A_g$ is due entirely to $\nu(C_aC_e)$ stretching in both the neutral parent and the anion and due to $\nu(C_aC_a)$ stretching in the dianion. The $26A_g$, $19A_g$, $17A_g$, $16A_g$, $14A_g$, $12A_g$, and $10A_g$ modes, all of which have large overlaps between different redox states, maintain the respective intrinsic stretching or bending modes. Fore example, $19A_g$ is due to $\nu(C_aN)$ stretching for every redox states (see Table 3 for other modes).

Since modes $20A_g$ to $25A_g$ exhibit less overlap between redox states as described above, complicated mode mixing occurs. The $25A_g$ mode includes $\nu(C_bC_b)$, but changes to $\nu_s(C_aC_bC_b)$ stretching in both the anion and dianion, whereas $23A_g$ includes $\nu_s(C_aNC_a)$, which appears to be the ν_4 mode for porphyrins, but changes to $\nu(C_bC_b)$ in the anion and to $\nu_s(C_bC_aC_e)$ in the dianion. The $21A_g$ mode includes $\nu(C_aN)$, and then changes to $\nu_s(C_bC_aC_e)$, and $20A_g$ is due to $\delta(HC_bC_b)$ bending, changing upon reduction to $\nu_{as}(C_aNC_a)$. Although both $18A_g$ and $19A_g$ include $\nu(C_aN)$ stretching, the former is due to the stretching of the pyrrole ring with N−H proton (pyrrole I), while the latter is due to the pyrrole ring without N−H proton (pyrrole II). This kind of mode separation was also observed for other modes, and the sets of normal modes ($22A_g$, $20A_g$), ($26A_g$, $27A_g$), and ($29A_g$, $28A_g$) exhibit basically similar displacement with either pyrrole I-localized or pyrrole II-localized vibrations.

Quantum chemical calculations revealed that the bond lengths varied alternately around the porphycene ring after the first reduction. Thus, it appears reasonable that the frequency shift of a particular mode should follow the variation in bond lengths related to the mode. The lower frequency shifts of the Raman bands at 1606, 1542, and 1498 cm^{-1} involving $\nu(C_aC_a)$, $\nu(C_aC_e)$, and $\nu(C_bC_b)$ stretching in both the neutral parent and the anion are consistent with the increase in C_aC_a, C_aC_e, and C_bC_b bond lengths in the anion state. Other downshifts of Raman bands at 1430 and 1398 cm^{-1} involving $\nu(C_bC_b)$ stretching also appear to be consistent with the elongation of the C_bC_b bond and the minor change in the C_aN bond upon reduction. The shortening of the C_eC_e bond supports the upshifts observed for two Raman bands observed at 1559 and 1159 cm^{-1}, both of which involve $\nu(C_eC_e)$ stretching. The small frequency shift of the 1259 and 1202 cm^{-1} bands appears to be consistent with the very small change in the C_aN bond. It is, however, difficult to explain the frequency shifts of bending modes qualitatively regardless of any good match between the experimental and theoretical behavior. The frequency shift patterns observed after the first reduction can therefore be rationalized in terms of structural changes initiated by an excess electron in the LUMO of the neutral parent if the orthogonality of each normal mode is preserved across redox states.

The bond lengths change as a result of the second reduction in a manner similar to that from the first reduction. The continuous shifts indicate that the vibrational characteristics of the normal modes are preserved upon reduction, for example $26A_g$ (85−86% overlap) and $19A_g$ (92−96% overlap). Generally, however, vibrational mode mixing will promote mixed upshifts and downshifts, implying significant alteration of the mode compositions in different redox states. Such shifts were observed for the $23A_g$, $25A_g$, and $30A_g$ modes, which all have very small overlaps. The $30A_g$ mode, for example, mixed considerably with $29A_g$ to give rise to an upshift in the dianion state, which can be explained by taking account of the contribution of $\nu(C_eC_e)$ stretching in the dianion state.

A variety of frequency shifts were observed for the skeletal vibrational modes of H_2Pc upon reduction, which is consistent with the vibrational analysis of porphycene. The behavior was analyzed qualitatively by considering alternating changes in bond lengths around the porphycene ring upon reduction, which appear to be a characteristic feature of the π-type anion and dianion.

Anion Radical and Its Dianion. Molecular orbital calculations suggest that the symmetry of both the anion and dianion porphycene is C_{2h}, which is consistent with the results recently reported by Kozlowski et al. for the neutral parent.[18] Those authors carried out molecular orbital calculations for neutral porphycene in various structural forms: trans (C_{2h}), cis (C_{2v}),

TABLE 3: Comparison of Experimental and Theoretical Results for RR Frequencies of Neutral Porphycene H_2Pc and the Anion and Dianion Forms ($\tilde{\nu}$/cm^{-1})

experimental			theoretical[a]							
			H_2Pc			anion		dianion		
H_2Pc freq	anion freq (Δ^b)	dianion freq (Δ^c)	mode	freq	displacement[d]	freq (Δ^b)	displacement[d]	freq (Δ^c)	displacement[d]
969	970 (+1)	972 (+2)	$10A_g$	969	NC_aC_b (44)	974 (+5)	NC_aC_b (45)	977 (+3)	NC_aC_b (46)
988[e]	991 (+3)	994 (+3)	$12A_g$	989	NC_aC_b (42)	996 (+7)	NC_aC_b (43)	1000 (+4)	NC_aC_b (42)
1063	1049 (−14)	1038 (−11)	$14A_g$	1061	C_bH (86)	1045 (−16)	C_bH (80)	1028 (−17)	C_bH (65)
1159	1168 (+9)	1166 (−2)	$16A_g$	1153	$C_aC_eC_eC_a$ (49)	1161 (+8)	$C_aC_eC_eC_a$ (40)	1160 (−1)	$C_aC_eC_eC_a$ (33)
1202	1195 (−7)	1195 (0)	$17A_g$	1208	C_aN (32)	1203 (−5)	C_aN (30)	1199 (−4)	C_aN (27)
1259	1259 (0)	1262 (+3)	$19A_g$	1271	C_aN (36)	1272 (+1)	C_aN (46)	1273 (+1)	C_aN (34)
1333	1315 (−18)		$20A_g$	1337	HC_bC_b (54)	1318 (−19)	C_aNC_a (38)	1303 (−15)	C_aNC_a (56)
1352	1338 (−14)	1356 (+18)	$21A_g$	1349	C_a**N** (41)	1343 (−6)	$C_bC_aC_e$ (32)	1355 (+12)	$C_bC_aC_e$ (41)
1398	1368 (−30)	1381 (+13)	$23A_g$	1396	C_aNC_a (46)	1376 (−20)	C_bC_b (29)	1382 (+6)	$C_bC_aC_e$ (46)
1430[e]	1401 (−29)	1415 (+14)	$25A_g$	1437	C_bC_b (47)	1418 (−19)	$C_aC_bC_b$ (57)	1424 (+6)	$C_aC_bC_b$ (52)
1498[e]	1467 (−31)	1455 (−12)	$26A_g$	1494	C_bC_b (34)	1467 (−27)	C_bC_b (32)	1445 (−22)	C_bC_b (21)
1542	1527 (−15)	1520 (−7)	$28A_g$	1543	C_aC_e (52)	1523 (−20)	C_aC_e (26)	1508 (−15)	C_aC_a (30)
1559	1564 (+5)	1573 (+9)	$29A_g$	1561	C_aC_e (52)	1562 (+1)	C_eC_e (59)	1568 (+6)	C_eC_e (35)
1606	1590 (−16)	1616 (+26)	$30A_g$	1604	C_aC_a (38)	1594 (−10)	C_aC_a (24)	1604 (+10)	C_eC_e (46)

[a] Multiple scaling factors were used for *trans*-H_2Pc, the anion, and dianion. [b] Frequency shifts between the neutral parent and the anion. [c] Frequency shifts between the anion and the dianion. [d] Values in parentheses are displacements of the focused atoms (see text). [e] Observed in the spectrum measured in CCl_4 (see Figure 1B).

SS-A (D_{2h}; two N−H protons laid on the long axis of the molecule bisecting the C_eC_e bond), and SS-B (D_{2h}; two N−H protons laid on the short axis of the molecule bisecting the C_aC_a bond), focusing on inner-hydrogen migration. At the B3LYP/6-31G(*d*) level, it was concluded on the basis of the energetics that the most favorable structure of the neutral porphycene is trans (C_{2h}). However, Möbius et al.[7] demonstrated in early work that the symmetry of the anion radical was D_{2h} on the ESR time scale. Their molecular orbital calculations also supported the finding of symmetrical N−H−N bonds in the porphycene core (SS-A). To solve this apparent contradiction, the present authors optimized the anion radical with the D_{2h} symmetry. The SS-A was energetically less stable than the trans form by 9.5 kcal/mol, and the energy of SS-B is 55.9 kcal/mol higher than SS-A. These results are comparable to 8.2 and 58.3 kcal/mol, respectively, for the neutral case.[17] Both SS structures of the anion gave rise to two imaginary vibrational modes, suggesting that these modes are transient states for synchronous double proton transfer as in the neutral porphycene. Details of the stability of various isomers of the anion and dianion with respect to inner-hydrogen migration will be presented in a forthcoming paper, along with real vibrational frequencies of the SS, which have never been matched to the observed RR frequencies rationalized previously by vibrational analysis for the trans structure (C_{2h}). However, the finding in the present analysis is that the anion radical of H_2Pc produced by the Na mirror technique has C_{2h} symmetry on a vibrational time scale, which is much shorter than the ESR time scale.

Since the HOMO of the dianion of H_2Pc is very similar to the LUMO of the neutral parent, two electrons will be introduced into the LUMO of the neutral parent upon reduction. The

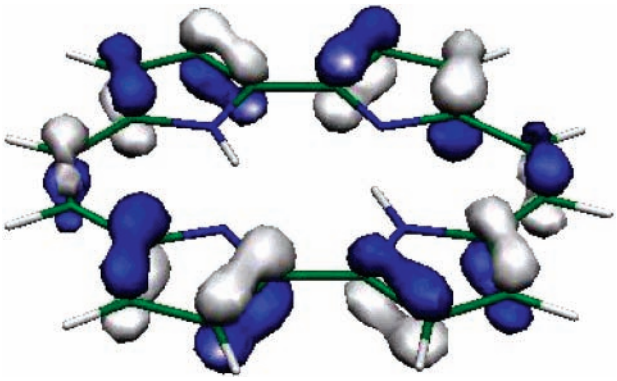

Figure 4. Top view of a HOMO of the H_2Pc dianion with trans C_{2h} symmetry.[26]

HOMO has π character with alternating node pattern, C_aC_b and C_eC_e bonding character, C_bC_b, C_aC_a, and C_aC_e antibonding character, and C_aN nonbonding, as shown in Figure 4. This kind of bond alternation is also observed for the e_g* orbital of porphyrins. However, in a specific bond, for example C_bC_b, all four of the constituent bonds have antibonding character for H_2Pc, whereas the bond has net antibonding character for porphyrins as governed by the topology. This may represent a characteristic feature of porphycene anions with respect to the electronic states.

Bocian et al. observed the RR spectra for the anion radical of a free-base porphyrin and reported reduction-induced frequency shifts.[13] These shifts were large for the peripheral vibrational modes but minor for the modes involving $\nu(C_aN)$, suggesting that the excess electron density in the porphyrin anion

was localized in the periphery of the macrocycle. Similar behavior was observed for the H_2Pc anions, as evidenced by the $17A_g$ and $19A_g$ modes involving $\nu(C_aN)$ stretching. In the case of porphycene anions, however, the HOMO nodal pattern is responsible for the small shifts of those modes because the C_aN bond has nonbonding character, as shown in Figure 4.

In conclusion, the present RR studies of the chemically generated anion radical and dianion species of H_2Pc, in conjunction with theoretical calculations, successfully resolved structural changes due to reduction. The observed frequency shifts generally agree well with the vibrational analysis of porphycene considering vibrational overlap in different redox states.

Acknowledgment. The authors thank Osaka City University for financial support. This work was supported in part by a Grant-in-Aid for Scientific Research (B) (Grant No.13554020) from Japan Society for the Promotion of Science. J.T. thanks Prof. Saburo Neya (Chiba University) for useful discussion.

References and Notes

(1) Vogel, E.; Köcher, M.; Schmickler, H.; Lex, J. *Angew. Chem., Int. Ed. Engl.* **1986**, *25*, 257−259.

(2) Vogel, E.; Balci, M.; Pramod, K.; Koch, P.; Lex, J.; Ermer, O. *Angew. Chem., Int. Ed. Engl.* **1987**, *26*, 928−931.

(3) Renner, M. W.; Forman, A.; Wu, W.; Chang, C. K.; Fajer, J. *J. Am. Chem. Soc.* **1989**, *111*, 8618−8621.

(4) Gisselbrecht, J. P.; Gross, M.; Köcher, M.; Lausmann, M.; Vogel, E. *J. Am. Chem. Soc.* **1990**, *112*, 8618−8620.

(5) Bernard, C.; Gisselbrecht, J. P.; Gross, M.; Vogel, E.; Lausmann, M. *Inorg. Chem.* **1994**, *33*, 2393−2401.

(6) Schlüpmann, J.; Huber, M.; Toporwicz, M.; Köcher, M.; Vogel, E.; Levanon, H.; Möbius, K. *J. Am. Chem. Soc.* **1988**, *110*, 8566−8567.

(7) Schlüpmann, J.; Huber, M.; Toporwicz, M.; Plato, M.; Köcher, M.; Vogel, E.; Levanon, H.; Möbius, K. *J. Am. Chem. Soc.* **1990**, *112*, 6463−6471.

(8) Ksenofontova, N. M.; Maslov, V. G.; Sidorov, A. N.; Bobovich, Ya. S. *Opt. Spectrosc.* **1976**, *40*, 462−465.

(9) Teraoka, J.; Hashimoto, S.; Sugimoto, H.; Mori, M.; Kitagawa, T. *J. Am. Chem. Soc.* **1987**, *109*, 180−184.

(10) Gurinovich, G. P.; Gurinovich, I. F.; Ivashin, N. V.; Sinyakov, G. N.; Shulga, A. M.; Terekhov, S. N.; Filatov, I. V.; Dzilinski, K. *J. Mol. Struct.* **1988**, *172*, 317.

(11) Atamian, M.; Donohoe, R. J.; Lindsey, J. S.; Bocian, D. F. *J. Phys. Chem.* **1989**, *93*, 2236−2243.

(12) Read, R. A.; Purrello, R.; Prendergast, K.; Spiro, T. G. *J. Phys. Chem.* **1991**, *95*, 9720−9727.

(13) Perng, J.-H.; Bocian, D. F. *J. Phys. Chem.* **1992**, *96*, 4804−4811.

(14) Hu, S.; Lin, C.-Y.; Blackwood, M. E.; Jr.; Mukherjee, A.; Spiro, T. G. *J. Phys. Chem.* **1995**, *99*, 9694−9701

(15) Lin, C.-Y.; Spiro, T. G. *Inorg. Chem.* **1996**, *35*, 5237−5243.

(16) Gulam, R. M.; Matsushita, T.; Neya, S.; Funasaki, N.; Teraoka, J. *Chem. Phys. Lett.* **2002**, *357*, 126−130.

(17) Malsch, K.; Hohlneicher, G. *J. Phys. Chem. A* **1997**, *101*, 8409−8416.

(18) Kozlowski, P. M.; Zgierski, M. Z.; Baker, J. *J. Chem. Phys.* **1998**, *109*, 5905−5913.

(19) Baker, J.; Jarzeck, A. A.; Pulay, P. *J. Phys. Chem. A* **1998**, *102*, 1412−1424.

(20) Lee, C.; Yang, W.; Parr, R. G. *Phys. Rev. B* **1988**, *37*, 785−789.

(21) Becke, A. D. *J. Chem. Phys.* **1993**, *98*, 5648−5652.

(22) Frisch, M. J.; Trucks, G. W.; Schlegel, H. B.; Scuseria, G. E.; Robb, M. A.; Cheeseman, J. R.; Zakrzewski, V. G.; Montgomery, J. A., Jr.; Stratmann, R. E.; Burant, J. C.; Dapprich, S.; Millam, J. M.; Daniels, A. D.; Kudin, K. N.; Strain, M. C.; Farkas, O.; Tomasi, J.; Barone, V.; Cossi, M.; Cammi, R.; Mennucci, B.; Pomelli, C.; Adamo, C.; Clifford, S.; Ochterski, J.; Petersson, G. A.; Ayala, P. Y.; Cui, Q.; Morokuma, K.; Malick, D. K.; Rabuck, A. D.; Raghavachari, K.; Foresman, J. B.; Cioslowski, J.; Ortiz, J. V.; Baboul, A. G.; Stefanov, B. B.; Liu, G.; Liashenko, A.; Piskorz, P.; Komaromi, I.; Gomperts, R.; Martin, R. L.; Fox, D. F.; Keith, T.; Al-Laham, M. A.; Peng, C. Y.; Nanayakkara, A.; Challacombe, M.; Gill, P. M. W.; Johnson, B.; Chen, W.; Wong, M. W.; Andres, J. L.; Gonzalez, C.; Head-Gordon, M.; Replogle, E. S.; Pople, J. A. *GAUSSIAN98*; Gaussian, Inc.: Pittsburgh, PA, 1998.

(23) Ditchfield, R.; Hehre, W. J.; Pople, J. A. *J. Chem. Phys.* **1971**, *54*, 724−728.

(24) Rauhut, G.; Pulay, P. *J. Phys. Chem.* **1995**, *99*, 3093−3100.

(25) Oertling, W. A.; Wu, W.; Lopez-Garriga, J. J.; Kim, Y.; Chang, C. K. *J. Am. Chem. Soc.* **1991**, *113*, 127−134.

(26) Flükiger, P.; Lüthi, H. P.; Portmann, S.; Weber, J. *MOLEKEL 4.0*; Swiss Center for Scientific Computing: Manno, Switzerland, 2000.